THE JOURNAL OF BIOLOGICAL CHEMISTRY VOL. 290, NO. 16, pp. 10535–10543, April 17, 2015

Synaptotagmin-1 Is an Antagonist for Munc18-1 in SNARE Zippering*

Received for publication, December 8, 2014, and in revised form, February 8, 2015 Published, JBC Papers in Press, February 25, 2015, DOI 10.1074/jbc.M114.631341

Xiaochu Lou[‡1], **Jaeil Shin**[‡1,2], **Yoosoo Yang**[§1], **Jaewook Kim**[§], **and Yeon-Kyun Shin**[‡§3]

From the [‡]*Department of Biochemistry, Biophysics and Molecular Biology, Iowa State University, Ames, Iowa 50011 and the* [§]*Biomedical Research Institute, Korea Institute of Science and Technology (KIST), Hwarangno 14-gil 6, Seongbuk-gu, Seoul 136-791, South Korea*

Background: The molecular mechanisms of the critical necessity of Munc18-1 protein for neurotransmitter release remain unclear.
Results: Synaptotagmin-1 competes with Munc18-1 in SNARE zippering and fusion pore opening.
Conclusion: Synaptotagmin-1 wins the tug-of-war in gaining control of the SNAREpin at the moment of membrane fusion.
Significance: This work clarifies an ambiguity concerning the Munc18-1 function in neuroexocytosis.

In neuroexocytosis, SNAREs and Munc18-1 may consist of the minimal membrane fusion machinery. Consistent with this notion, we observed, using single molecule fluorescence assays, that Munc18-1 stimulates SNARE zippering and SNARE-dependent lipid mixing in the absence of a major Ca^{2+} sensor synaptotagmin-1 (Syt1), providing the structural basis for the conserved function of Sec1/Munc18 proteins in exocytosis. However, when full-length Syt1 is present, no enhancement of SNARE zippering and no acceleration of Ca^{2+}-triggered content mixing by Munc18-1 are observed. Thus, our results show that Syt1 acts as an antagonist for Munc18-1 in SNARE zippering and fusion pore opening. Although the Sec1/Munc18 family may serve as part of the fusion machinery in other exocytotic pathways, Munc18-1 may have evolved to play a different role, such as regulating syntaxin-1a in neuroexocytosis.

Essential to the functional connectivity in the central nerve system is neurotransmitter release at synapses, which requires fusion of vesicles to the presynaptic plasma membrane. Vesicle fusion is an energetically costly process because it needs to overcome the energy barrier for merging two stable membranes to a single bilayer (1, 2).

The required fusion energy would have to be provided by the protein machinery. It is thought that SNAREs and Munc18-1 constitute the minimal fusion machinery (3, 4). The SNARE complex formed between vesicle SNARE (v-SNARE) and target plasma membrane SNARE (t-SNARE) is considered the core of the fusion machine (3–11). Further, the binding of Munc18-1 to the SNARE complex would provide an additional energetic boost in driving vesicle fusion (12–14).

There is ample evidence that SNAREs belong to the minimal fusion machinery. Treatment of the presynapse with the clostridial toxins, which specifically cleave SNARE proteins, abolishes neurotransmitter release completely (15–18). Furthermore, proteoliposomes reconstituted with SNAREs only support lipid mixing, demonstrating that SNAREs alone can drive membrane fusion (8, 19–24). Similarly, it was shown that Munc18-1 accelerates SNARE-mediated proteoliposome fusion, supporting the notion that Munc18-1 is part of the minimal fusion machine (12, 25).

Meanwhile, Munc18-1 appears to have another important function to regulate the SNARE assembly. Munc18-1 binds to the Habc domain of t-SNARE syntaxin-1a and prevents sytaxin-1a from the premature binding to another t-SNARE, SNAP-25, which might lead to a nonproductive t-SNARE complex (26–30).

Although the Munc18-1 function to protect syntaxin-1a is supported by a variety of evidence, its role as part of the fusion machine is debatable. The proteoliposome fusion assay (12, 25), on which this proposition relies heavily, did not include synaptotagmin-1 (Syt1),[4] a major Ca^{2+} sensor for synaptic vesicle fusion (31–33). Syt1 is a vesicular protein, consisting of tandem Ca^{2+}-binding C2 domains and a transmembrane helix (34). Syt1 interacts with the core SNARE complex as well as phospholipids (35–39). Provided that Syt1 cooperates with the SNARE complex intimately during the moment of fusion, it is difficult to envision how Munc18-1 might gain access to the core complex simultaneously (40).

In this work, we investigated, using single molecule FRET (smFRET), the conformational changes of a *trans*-SNARE com-

* This work was supported, in whole or in part, by National Institutes of Health Grant R01 GM051290 (to Y.-K. S.). This work was also supported by Korea Institute of Science and Technology (KIST) Institutional Project 2E25520.
[1] These authors contributed equally to this work.
[2] Present address: Dept. of Molecular Biosciences and Howard Hughes Medical Institute, Northwestern University, Evanston, IL 60208.
[3] To whom correspondence should be addressed: Dept. of Biochemistry, Biophysics and Molecular Biology, Mol-Biol 4152, Iowa State University, Ames, IA 50011. Tel.: 515-294-2530; E-mail: colishin@iastate.edu.

[4] The abbreviations used are: Syt1, synaptotagmin-1; smFRET, single molecular FRET; t- and v-disc, t- and v-SNARE-reconstituted nanodisc, respectively; t- and v-vesicle, t- and v-SNARE-reconstituted vesicle, respectively; NN, N-terminal FRET pair; CC, C-terminal FRET pair; OG, octyl β-D-glucopyranoside; biotin-DPPE, 1,2-dipalmitoyl-*sn*-glycero-3-phosphoethanolamine-*N*-(biotinyl); biotin-PEG-DSPE, 1,2-distearoyl-*sn*-glycero-3-phosphoethanolamine-*N*-(biotinyl(polyethylene glycol)-2000); DOPS, 1,2-dioleoyl-*sn*-glycero-3-phospho-L-serine; POPC, 1-palmitoyl-2-oleoyl-*sn*-glycero-3-phosphocholine; PIP_2, phosphatidylinositol 4,5-bisphosphate; DiI, 1,1′-Dioctadecyl-3,3,3′,3′-tetramethylindocarbocyanine perchlorate; DiD, 1,1′-dioctadecyl-3,3,3′,3′-tetramethylindodicarbocyanine perchlorate; TIRF, total internal reflection fluorescence; SRB, sulforhodamine B.

plex (or SNAREpin) assembled between two nanodisc membranes (41) induced by Munc18-1. We also studied the effect of Munc18-1 on SNARE-dependent proteoliposome lipid mixing and on the Ca^{2+}-triggered fusion pore opening in well defined *in vitro* settings (39, 42) to dissect the Munc18-1 function in the presence of Syt1. Our results show that although Munc18-1 has the capacity to stimulate SNARE complex formation and SNARE-dependent lipid mixing, Syt1 largely negates such positive effects on membrane fusion, suggesting that Syt1 acts as an antagonist for Munc18-1.

EXPERIMENTAL PROCEDURES

Plasmid Constructs and Site-directed Mutagenesis—DNA sequences encoding rat syntaxin-1a (amino acids 2–288 with three native cysteines (Cys-145, -271, and -272) replaced by alanines), rat VAMP2 (amino acids 1–116 with Cys-103 replaced by alanine), soluble rat VAMP2 (Vps, amino acids 1–94), and rat SNAP-25 (amino acids 1–206 with four native cysteines (Cys-85, -88, -90, and -92) replaced by alanines) were inserted into the pGEX-KG vector as N-terminal glutathione *S*-transferase (GST) fusion proteins. Full-length rat Syt1 (amino acids 50–421 with four native cysteines (Cys-74, -75, -77, and -79) replaced by alanines and another cysteine (Cys-82) replaced by serine) and full-length rat Munc18-1 were inserted into pET-28b vector as C-terminal His-tagged proteins. We used the QuikChange site-directed mutagenesis kit (Stratagene) to generate all mutants, including syntaxin-1a I203C and V241C and VAMP2 Q33C and A72C. DNA sequences were confirmed by the Iowa State University DNA Sequencing Facility.

Protein Expression and Purification—Protein expression and purification were described previously (41, 43). Briefly, all recombinant proteins were expressed in *Escherichia coli* BL21 (DE3). GST-tagged proteins, syntaxin-1a, SNAP-25, VAMP2, and Vps were purified by affinity chromatography using glutathione-agarose beads (Sigma-Aldrich) and were cleaved from beads with thrombin (0.02 unit μl^{-1}; Sigma-Aldrich) in PBS or PBS with 0.8% (w/v) octyl β-D-glucopyranoside (PBS-OG) for membrane proteins. His-tagged proteins, apoA1, Syt1, and Munc18-1 were purified by nickel-nitrilotriacetic acid-agarose beads (Qiagen). His-tagged apoA1 and Munc18-1 were eluted with 200 mM imidazole (Sigma-Aldrich) in PBS. Munc18-1 was further dialyzed in 2 liters of PBS buffer at 4 °C overnight after elution. Syt1 was eluted with 25 mM HEPES, pH 7.4, with buffer containing 400 mM KCl, 250 mM imidazole, 0.8% OG, and 1 mM EDTA.

Lipid Mixture Preparation—The lipid molecules used in this study are 1,2-dioleoyl-*sn*-glycero-3-phospho-L-serine (DOPS), 1-palmitoyl-2-oleoyl-*sn*-glycero-3-phosphocholine (POPC), phosphatidylinositol 4,5-bisphosphate (PIP_2; from porcine brain), cholesterol, 1,2-dipalmitoyl-*sn*-glycero-3-phosphoethanolamine-*N*-(biotinyl) (biotin-DPPE), and 1,2-distearoyl-*sn*-glycero-3-phosphoethanolamine-*N*-(biotinyl(polyethylene glycol)-2000) (biotin-PEG-DSPE). All lipids were obtained from Avanti Polar Lipids. 1,1′-Dioctadecyl-3,3,3′,3′-tetramethylindocarbocyanine perchlorate (DiI), 1,1′-dioctadecyl-3,3,3′,3′-tetramethylindodicarbocyanine perchlorate (DiD), and sulforhodamine B were obtained from Invitrogen. The desired amounts of lipids were first mixed in a glass tube, and the mixture was then completely dried under vacuum.

Fluorophore Labeling of the Single Cysteine Mutants—The fluorophore labeling of the single cysteine mutants of syntaxin-1a and VAMP2 was described previously (41, 44). Briefly, the mutants were purified as described above for syntaxin-1a and VAMP2 except that the cleavage buffer contained 2.5 mM DTT. For smFRET of the *trans*-SNAREpin, cysteine mutants of syntaxin-1a (I203C or V241C) and VAMP-2 (Q33C or A72C) were desalted with the PD-10 column (GE Healthcare) to eliminate free DTT and then incubated with a 10-fold molar excess of maleimide-derivative fluorophores Cy5 and Cy3 (GE Healthcare), respectively, at 4 °C overnight. Unreacted free fluorescence labels were removed by the PD-10 column. The labeling efficiency of each mutant was measured with spectrophotometry (Beckman). Extinction coefficients of Cy5 (250,000 M^{-1} cm^{-1} at 650 nm) and Cy3 (150,000 M^{-1} cm^{-1} at 552 nm) were used to calculate concentrations of fluorophores. The detergent-compatible Lowry assay (DC assay, Bio-Rad) was used to determine the protein concentration. The labeling efficiencies were 46 and 40% for syntaxin-1a I203C and V241C, whereas they were 55 and 62% for VAMP2 Q33C and A72C, respectively.

Reconstitution and Purification of t- and v-discs—The mixture of POPC, DOPS, cholesterol, PIP_2, and biotin-PEG-DSPE with a molar ratio of 62.9:15:20:2:0.1 for t-discs and the mixture of POPC, DOPS, and cholesterol with a molar ratio of 75:5:20 for v-discs were dried and resuspended in Tris150-EDTA buffer (10 mM Tris-HCl, 150 mM NaCl, 1 mM EDTA, pH 7.4). The lipid compositions were chosen to emulate those of the presynaptic and the vesicle membranes at least for major lipid components. 3 μl of each 50 mM lipid mixture was dissolved in sodium cholate (final concentration of 50 mM). Then t-SNARE (the binary complex of syntaxin-1a and SNAP-25) or v-SNARE (VAMP-2 with or without Syt1 with a molar ratio of 1:1) and apoA1 protein were added to the detergent-solubilized lipid mixture. The molar ratio of lipid, SNARE(s), and apoA1 was 160:0.5:2. The self-assembly of SNARE-incorporated nanodiscs was initiated by the rapid removal of sodium cholate by treating the sample with 50% (w/v) SM-2 Bio-Beads (Bio-Rad). The t- or v-discs were then purified through gel filtration using a Superdex™ 200 GL 10/30 column (Amersham Biosciences).

FRET Measurements of trans-SNAREpins—After coating the quartz surface with a solution of methoxy-polyethylene glycol and biotin-PEG molecules (100:1), the quartz slide was assembled into a flow chamber and coated with streptavidin (0.2 mg ml^{-1}). The t-discs containing Cy5-labeled sytnaxin-1a) were immobilized on the surface by flowing in 100–200 nM nanodisc solution. Then 1 μM Munc18-1 or an equal volume of buffer was injected in, and the sample was incubated for 10 min at room temperature (~25 °C). A 5-fold molar excess of v-discs containing Cy3-labeled VAMP2 without or with Syt1 with 1 μM Munc18-1 or an equal volume of buffer was then added to the flow chamber, and the sample was incubated for 25 min at 37 °C to allow *trans*-SNAREpin formation. All total internal reflection experiments were performed at room temperature in the presence of the oxygen scavenger system (0.4% (w/v) glucose (Sigma), 4 mM Trolox (Calbiochem), 1 mg/ml glucose oxidase (Sigma), 0.04 mg/ml catalase (Calbiochem)) in Tris150-EDTA

buffer. The smFRET measurements were carried out on a prism-type total internal reflection fluorescence (TIRF) setup, which is based on the inverted microscope (IX71, Olympus) with the laser exposure time of 200 ms. A solid-state laser at 532 nm was used to excite the Cy3-labeled v-discs and measure FRET, and a helium-neon (HeNe) laser at 635 nm was used to check the presence of the Cy5-labeled t-discs. The Cy3 and Cy5 fluorescence emissions were collected by a water immersion lens (UPlanSApo 60×/1.20w, Olympus) and split by a dichroic mirror (T660lpxr, Chroma), which has a threshold at the 635 nm wavelength. Both Cy3 and Cy5 emissions were then imaged with the imaging area of $45 \times 90\ \mu m^2$ side by side on an electron-multiplying charged-coupled device camera (iXon DU897E, Andor Technology), which has high quantum efficiency in the 450–700 nm range. The collected images were analyzed by smCamera (kindly provided by Dr. Taekjip Ha's group). FRET efficiencies (E) were obtained by the following,

$$E = \frac{I_A}{(I_A + I_D)} \quad \text{(Eq. 1)}$$

where I_A and I_D represent the acceptor and donor fluorescence intensities. More details about the experimental setup can be found in a recent review paper (45), and representative traces can be found in our previous work (Fig. 4 in Ref. 41).

Proteoliposome Reconstitution—For the bulk and single lipid mixing assays, the molar ratios of lipids were 15:62:20:2:1:0.1 (DOPS/POPC/cholesterol/PIP_2/DiI/biotin-DPPE) for the t-SNARE-reconstituted vesicles (t-vesicles) and 5:74:20:1 (DOPS/POPC/cholesterol/DiD) for the v-SNARE-reconstituted vesicles (v-vesicles), respectively. For the t-vesicles without PIP_2, an equal molar amount of POPC was used instead. The lipid mixture was first completely dried under vacuum and then hydrated by dialysis buffer (25 mM HEPES, pH 7.4, 100 mM KCl). After five freeze-thaw cycles, protein-free large unilamellar vesicles (~100 nm in diameter) were prepared by extrusion through a 100-nm polycarbonate filter (Whatman). For membrane reconstitution, SNARE proteins and Syt1 were mixed with protein-free vesicles at a protein/lipid molar ratio of 1:200 for each protein component (this ratio was kept for all experiments, including the single vesicle content mixing assay) with 0.8% OG in the dialysis buffer at 4 °C for 15 min. The liposome/protein mixture was diluted 2 times with dialysis buffer for t-vesicles, and then the diluted t-vesicles were dialyzed in 2 liters of dialysis buffer at 4 °C overnight. For v-vesicles, the mixture was diluted twice with dialysis buffer containing 1 mM EDTA and dialyzed in 2 liters of dialysis buffer with EDTA at 4 °C overnight. Details for reconstitution were described in our previous work (39, 43).

For the single vesicle content-mixing assay with the small sulforhodamine B content indicator, the lipid compositions were the same as those used in the single vesicle docking assay except that the fluorescent lipid dyes (DiI and DiD) were replaced by an equal amount of POPC, and 2% PIP_2 was incorporated into the t-vesicles. The lipid mixture was first completely dried and then hydrated with dialysis buffer. A population of vesicles intended for v-vesicles was hydrated in the presence of 20 mM sulforhodamine B (SRB). The overall vesicle preparation and protein reconstitution process was the same as above except that v-vesicles were always kept throughout in the 20 mM SRB prior to dialysis overnight. Remaining free SRB was removed using the PD-10 desalting column (GE Healthcare) after dialysis. Details for reconstitution were described in our previous work (39, 43).

Single Vesicle Docking and Lipid-mixing Assays—The t-vesicles with a final lipid concentration of 1 μM were flowed into the chamber and immobilized on the PEG-coated surface through the streptavidin-to-biotin lipid conjugation with a 30-min incubation at room temperature (~25 °C). After two rounds of washing with 200 μl of dialysis buffer, 1 μM Munc18-1 or an equal volume of dialysis buffer was flowed into the chamber, and the sample was incubated for another 30 min at room temperature. Then the v-vesicles (3 μM) with or without 1 μM Munc18-1 were injected into the flow chamber, and the sample was again incubated for 30 min at 37 °C. After washing off free v-vesicles using dialysis buffer containing 1 μM Munc18-1 or an equal volume of dialysis buffer, movies were acquired by taking 100 consecutive frames with the 100-ms exposure time from five randomly chosen imaging areas using the same TIRF setup described above. The first 60 frames were taken by using 532-nm laser excitation for DiI-labeled t-vesicles, and these data were used to calculate the FRET efficiency, and the following 40 frames were taken by using 635-nm laser excitation to verify the presence of DiD-labeled v-vesicles. The nonspecifically bound v-vesicles were excluded from the analysis.

Single Vesicle Content-mixing Assay—The t-SNARE vesicles (125 μM) were immobilized on the PEG-coated surface through the streptavidin-to-biotin lipid conjugation for 20 min. Following several rounds of washing with 200 μl of dialysis buffer, the v-vesicles containing 20 mM SRB (10 μM) were injected into the flow chamber, and the sample was incubated at room temperature for 10 min for docking. After washing out the unbound v-vesicles with dialysis buffer containing 1 mM EDTA, an additional 20-min incubation was followed by the injection of 500 μM Ca^{2+} using the motorized syringe pump. Movies were acquired using the same TIRF setup as described above with 532-nm excitation for SRB, and the stepwise jump in the fluorescence emission intensity due to fluorescence dequenching of SRB was recorded as the signal for content mixing; the representative images and traces can be found in our previous work (see Fig. S2 in Ref. 39 and Figs. 1*B* and S6*B* in Ref. 43). The details of TIRF microscope imaging and the data analysis of the single vesicle content mixing assay were described in detail elsewhere (46).

RESULTS

Munc18-1 Promotes SNARE Zippering without Syt1 but Not in the Presence of Syt1—It has been shown previously that Munc18-1 can bind to the SNARE four-helix bundle, but it has not yet been demonstrated that such binding actually stimulates SNARE zippering (47). To investigate the effects of Munc18-1 on the conformation of the *trans*-SNAREpin with smFRET, we prepared the N-terminal FRET pair VAMP2 Q33C and syntaxin-1a I203C labeled with the donor dye Cy3 and the acceptor dye Cy5, respectively (NN). We also prepared a C-terminal FRET pair, Cy3-labeled VAMP2 A72C and Cy5-labeled syntaxin-1a V241C (CC) (Fig. 1*A*). For the detection of FRET with TIRF microscopy, the t-SNARE-reconstituted nano-

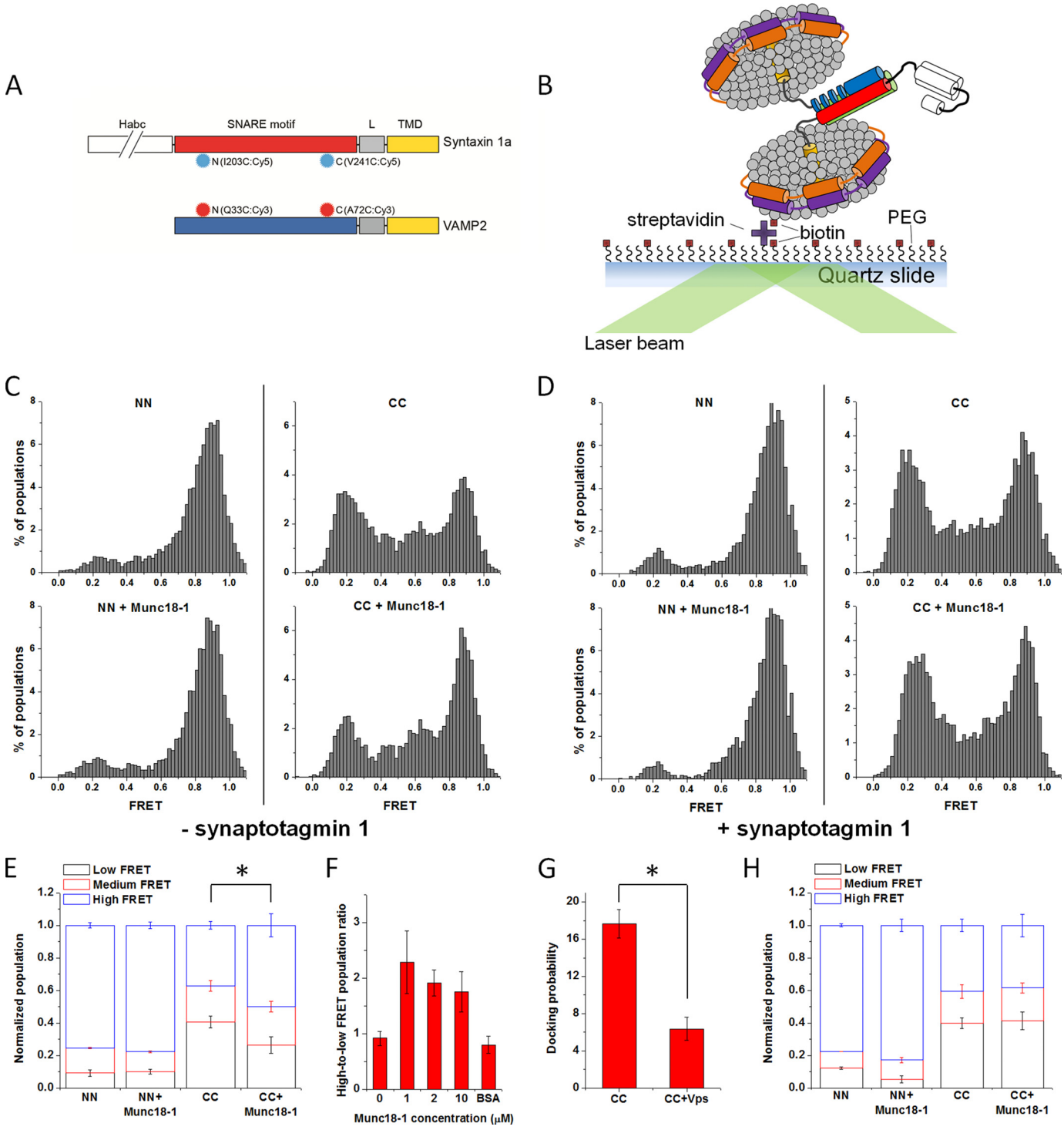

FIGURE 1. **Effects of Munc18-1 on the conformation of the *trans*-SNAREpin detected by smFRET.** *A*, fluorescent dye-labeled positions on syntaxin-1a and VAMP2. I203C or V241C of syntaxin-1a was labeled with Cy5 (*light blue saw tooth circle*), and Q33C or A72C of VAMP2 was labeled with Cy3 (*red saw tooth circle*). The Habc domain (*white*) of syntaxin-1a is depicted as *broken* to indicate the longer length than the SNARE motif (*red*). *B*, the TIRF microscope setup for the smFRET detection of the *trans*-SNAREpin conformation. The t-discs carrying Cy5-labeled syntaxin-1a (*red* and *white*) and SNAP-25 (*green*) were immobilized on the quartz surface through the biotin (*yellow square*) and streptavidin (*purple cross*) conjugation and then allowed to interact and form the *trans*-SNAREpin with the v-discs carrying Cy3-labeled VAMP2 (*blue*) with or without Syt1 (not shown). Distributions of the FRET efficiency for the NN and CC in the absence (*top*) or presence (*bottom*) of Munc18-1 without Syt1 (*C*) and with Syt1 (*D*), respectively. *E*, plot of the normalized FRET populations in the absence of Syt1 using the cut-off FRET efficiencies (*E*) of $E \leq 0.4$ for low FRET, $0.4 < E < 0.72$ for medium FRET, and $E \geq 0.72$ for high FRET. *F*, the relative changes in the ratio of high to low FRET populations for the CC in the presence of increasing amount of Munc18-1 or 2 μM BSA without Syt1. *G*, docking ability of the CC in the absence and presence of 10 μM soluble VAMP2 (Vps, amino acids 1–94). *H*, plot of the normalized FRET populations in the presence of Syt1 using the cut-off FRET efficiencies (*E*) of $E \leq 0.4$ for low FRET, $0.4 < E < 0.72$ for medium FRET, and $E \geq 0.72$ for high FRET. *Error bars*, S.D. of three independent experiments; movies were recorded for the analysis from more than five randomly selected screens in each experiment. *, $p < 0.05$, assessed using the two-sample Student's *t* test unless otherwise specified.

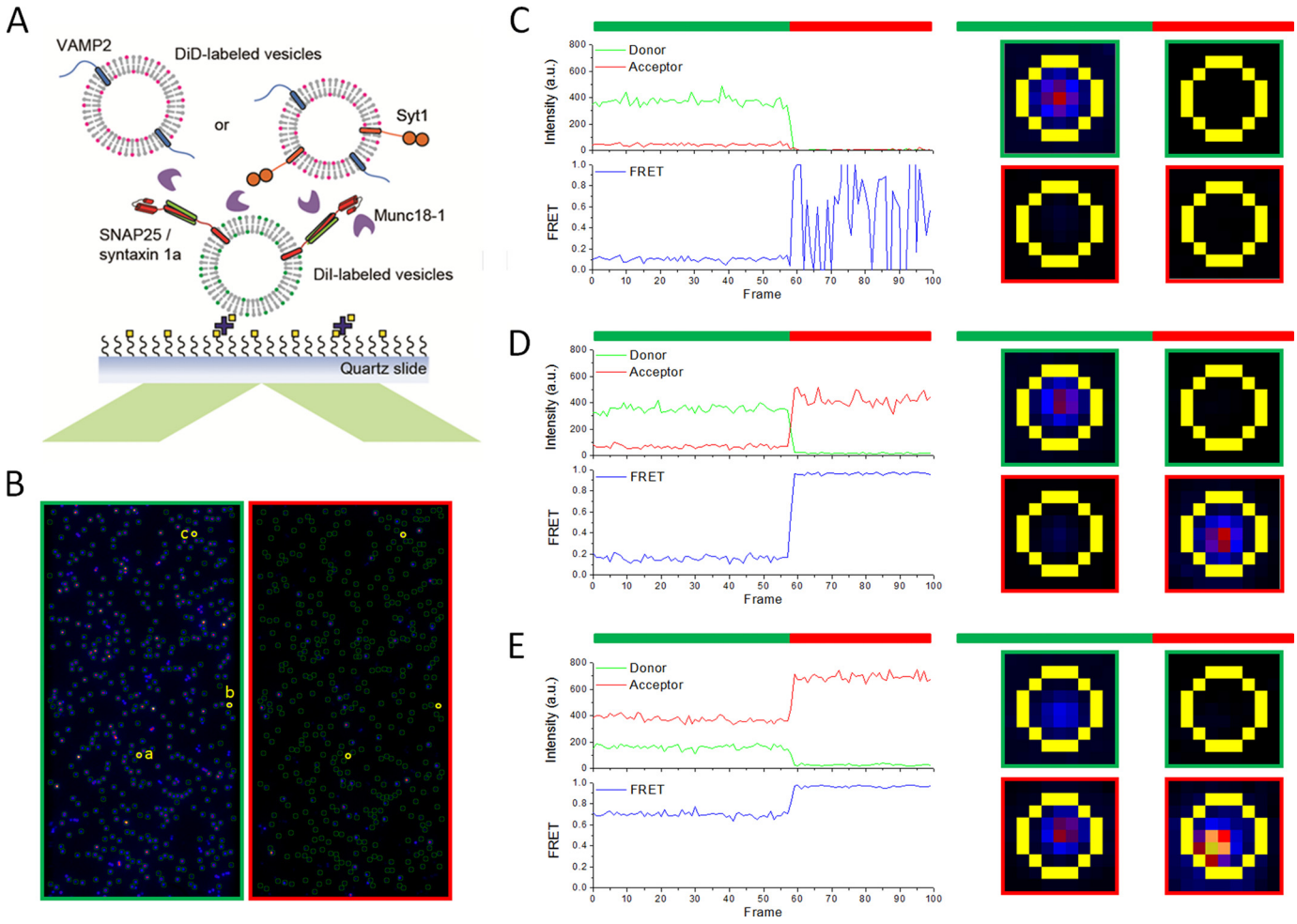

FIGURE 2. **Schematic diagram and representative traces of the single vesicle docking and lipid mixing assay.** *A*, schematic diagram of the single vesicle docking and lipid mixing assay. t-vesicles reconstituted with SNAP-25/syntaxin-1a were immobilized on the surface of the flow cell. v-vesicles reconstituted with VAMP2 or VAMP2 together with Syt1 (VAMP2/Syt1 = 1:1) were flowed into the flow cell with or without 1 μM Munc18-1. *B*, representative imaging areas of DiI (*green-framed*, *left*) and DiD (*red-framed*, *right*) emission under 532-nm excitation for DiI-labeled t-vesicles. Each *green circle* on the *left* represents emission from an immobilized t-vesicle, and the fluorescence emission was analyzed as shown on the *right*. Three representative spots were chosen as shown in *yellow* circles and *labeled a*, *b*, and *c*. *C*, the *trace* of *spot a* represents immobilized t-vesicle only. *D*, the *trace* of *spot b* represents docking of v-vesicle onto the immobilized t-vesicle without significant lipid mixing. *E*, the *trace* of *spot c* represents docking of the v-vesicle onto the immobilized t-vesicle with significant lipid mixing. *Green bar*, 532-nm excitation for FRET; *red bar*, 635-nm excitation for checking the presence of docked vesicles.

discs (t-discs) were tethered on the imaging surface using the streptavidin-to-biotin lipid conjugation. The v-SNARE-reconstituted nanodiscs (v-discs) were then flowed into the flow cell to allow docking and *trans*-SNAREpin formation (Fig. 1*B*) (41).

For the SNAREpin with the NN, we observed a dominant FRET distribution peaking at the FRET efficiency E ~0.9 (Fig. 1*C*, *left*), indicating that the helical structure is robust at the N-terminal region. We observed a small low FRET population (~8%) that might reflect nonspecific binding of nanodiscs on the surface (Fig. 1*C*, *left*). The possibility of antiparallel SNARE assembly (48) could be ruled out because out-of-register combinations (NC and CN) populated mid-FRET dominantly (E ~0.4) (see Fig. 2*C* in Ref. 41), but we did not observe an appreciable mid-FRET population for the NN. In contrast, the SNAREpin with the CC gave two major low and high FRET distributions with some population at mid-FRET (Fig. 1*C*, *top right*; see Ref. 41 for a discussion of the mid-FRET population). The low FRET peak might reflect a half-zipped SNAREpin, whereas the high and mid FRET peaks represent a fully zipped SNAREpin (41). When Munc18-1 (1 μM) was added, for the CC, we observed the shift of the FRET distribution from low to high, reflecting that Munc18-1 promoted formation of the fully zipped SNAREpin (Fig. 1, *C* (*bottom right*) and *E*), which was a Munc18-1-dependent instead of nonspecific packing effect (Fig. 1*F*). The association between a t-disc and a v-disc was SNARE-dependent, as evidenced by the significant reduction of the association in the presence of soluble VAMP2 (Fig. 1*G*).

Now, to find out whether such a promotion of SNARE zippering by Munc18-1 still happens in the presence of Syt1, we incorporated Syt1 into the v-disc in a molar ratio of 1:1 to VAMP2. With Syt1, we still observed a dominant high FRET distribution for the NN (Fig. 1*D*, *top left*), identical to that observed in the absence of Syt1. Interestingly, however, we did not observe any change in the distribution of the CC population at all (Fig. 1, *D* (*right*) and *H*). Thus, the results suggest that Syt1 works as an antagonist to Munc18-1 to interact with SNAREpin, which abrogates the enhancement of SNARE zippering by Munc18-1.

Syt1 and Munc18-1 Are Mutually Antagonistic in SNARE-dependent Lipid Mixing—Because Munc18-1 stimulated SNARE zippering in the absence of Syt1, we tested whether

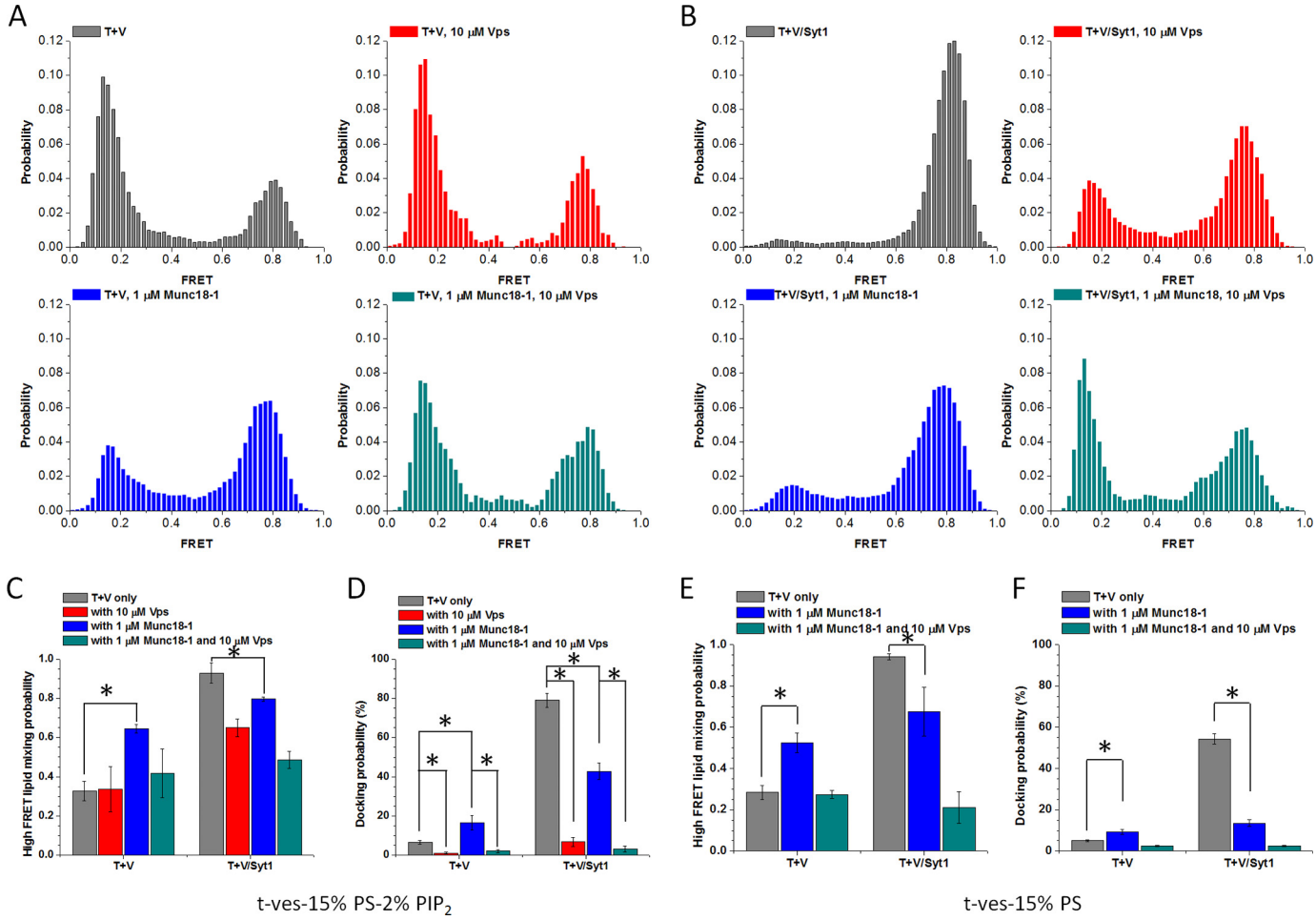

FIGURE 3. **Munc18-1 and Syt1 are mutually antagonistic in SNARE-dependent lipid mixing.** *A*, normalized distributions of FRET efficiencies for immobilized t-vesicles and docked VAMP2-vesicles (*gray*), VAMP2-vesicles in the presence of 10 μM Vps (*red*), VAMP2-vesicles in the presence of 1 μM Munc18-1 (*blue*), and VAMP2-vesicles in the presence of 10 μM Vps and 1 μM Munc18-1 (*dark cyan*). *B*, normalized distributions of FRET efficiencies for immobilized t-vesicles and docked VAMP2/Syt1-vesicles (*gray*), VAMP2/Syt1-vesicles in the presence of 10 μM Vps (*red*), VAMP2/Syt1-vesicles in the presence of 1 μM Munc18-1 (*blue*), and VAMP2/Syt1-vesicles in the presence of 10 μM Vps and 1 μM Munc18-1 (dark *cyan*). *C*, lipid-mixing efficiencies quantified based on the percentages of normalized high FRET population ($E \sim 0.5$–1) (65). *Bars* are normalized with respect to the number of the docked vesicles to take into account the differences in docking probabilities (*D*). *E*, lipid-mixing efficiencies quantified based on the percentages of the normalized high FRET population ($E \sim 0.5$–1) (65) for the t-vesicles without PIP_2. *Bars* are normalized with respect to the number of the docked vesicles (*F*). *Error bars*, S.D. of three independent experiments; movies were recorded for analysis from more than five randomly selected screens in each experiment. *, $p < 0.05$, assessed using the two-sample *t* test, unless otherwise specified.

Munc18-1 could stimulate lipid mixing, as was previously observed by Rothman and co-workers (12). To measure lipid mixing with the single vesicle assay, we immobilized vesicles carrying t-SNARE on the imaging surface (t-vesicles), and vesicles carrying v-SNARE (v-vesicles) were added to the flow cell to allow vesicle docking (Fig. 2*A*). The lipid dyes DiI and DiD were separately incorporated into t- and v-vesicles, respectively, to detect FRET due to lipid mixing (Fig. 2, *B*–*E*). Without Munc18-1, lipid mixing was slow; only around 30% of docked vesicles showed lipid mixing after 30 min of incubation (*gray bars* in Fig. 3, *A* and *C*). However, when Munc18-1 was present, lipid mixing was accelerated significantly; 65% of docked vesicles were lipid-mixed (*blue bars* in Fig. 3, *A* and *C*), consistent with results reported previously (14). Moreover, we observed that Munc18-1 could also stimulate the docking between v-vesicles and t-vesicles, which is SNARE-dependent (Fig. 3*D*).

On the other hand, when Syt1 was incorporated into the v-vesicles in a molar ratio of 1:1 to VAMP2, we observed great enhancement of lipid mixing. After 30 min of incubation, nearly all docked vesicles were lipid-mixed (*gray bars* in Fig. 3, *B* and *C*). The stimulation of SNARE-dependent lipid mixing and vesicle docking by Syt1 (Fig. 3*D*) was reported previously (39) and was not surprising. However, what was surprising was that when we added Munc18-1, the stimulation of SNARE-dependent vesicle docking and lipid mixing by Syt1 was reduced. We observed about 80% of docked vesicles to have lipid mixing (*blue bars* in Fig. 3, *B* and *C*), and the docking was reduced by as much as 50% (Fig. 3*D*). Because both SNARE and PIP_2 were known to be important for the Ca^{2+}-independent vesicle docking and lipid mixing, we removed PIP_2 from t-vesicles. Without PIP_2, Munc18-1 behaved the same as it did when PIP_2 was present (Fig. 3, *E* and *F*), and the docking was reduced even further by as much as 70% (Fig. 3*F*) in the presence of Syt1. Therefore, our results suggest that Munc18-1 is again antagonistic to Syt1 in SNARE-dependent vesicle docking and lipid mixing.

Munc18-1 Has Little Effect on Ca^{2+}-triggered Content Mixing—Although SNAREs alone as well as SNAREs together with Syt1 can support lipid mixing, they are not effective in driving content mixing or fusion pore formation unless Ca^{2+} is

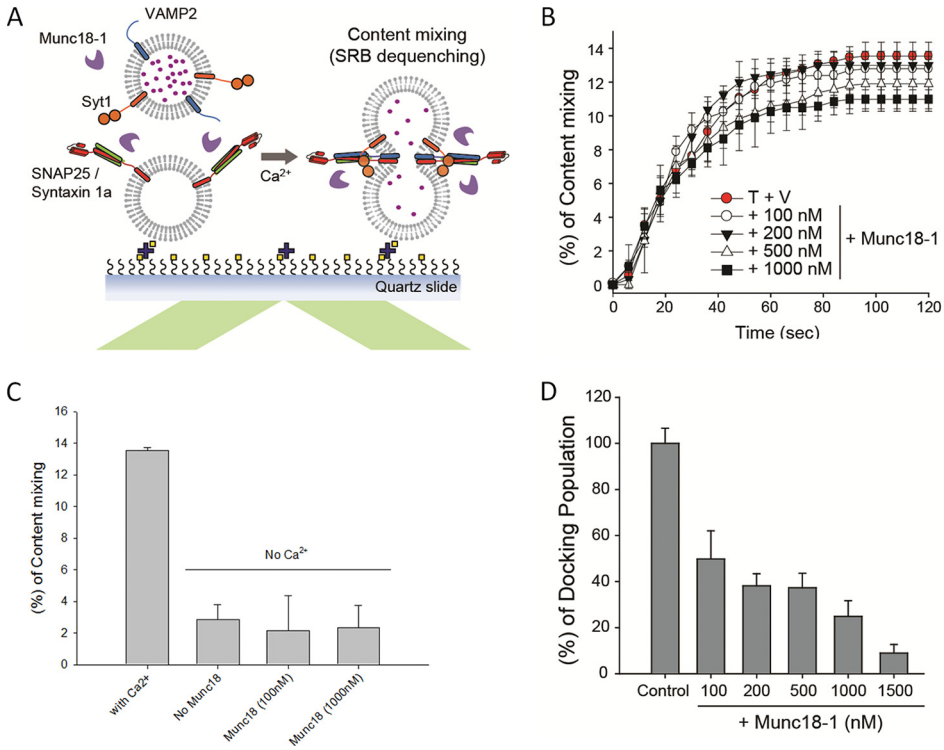

FIGURE 4. **Effects of Munc18-1 on Ca^{2+}-triggered fusion pore opening in *in vitro* content mixing assay.** *A*, schematics of the *in vitro* content mixing assay. *B*, quantitative comparison of the cumulative time content mixing percentage of the total docked population at various concentrations of Munc18-1 (Ca^{2+} injection at 10 s). The control, without Munc18-1, is depicted with *red circles*. *C*, plot of the content mixing percentage at 120 s in the absence of Ca^{2+}. *D*, *in vitro* single vesicle docking. Individual v-vesicles that tethered onto the t-vesicles on the imaging area were counted. The experiments were performed by incubating the samples in the presence of the specified Munc18-1 concentrations. The data were normalized against the control, which was obtained in the absence of Munc18-1. *Error bars* in *B–D*, S.D. of three independent experiments; a movie was recorded for analysis from one randomly selected screen in each experiment.

present (39, 43). As such, an *in vitro* Ca^{2+}-triggered content mixing assay offers a more stringent test for the competition between Munc18-1 and Syt1 to gain access to the SNAREpin.

To measure content mixing, we incorporated sulforhodamine B into the v-vesicles in an *in vitro* setup depicted in Fig. 2*A* except for lipid dyes (Fig. 4*A*). After vesicle docking, Ca^{2+} (500 μM) was flowed into the flow cell, and the intensity jump of the fluorescence signal due to fluorescence dequenching was detected as a signal for content mixing (43). The cumulative time plot shows that ~13.5% of docked vesicles undergo content mixing with a half-time of ~30 s (Fig. 4*B*), which is both Syt1- and SNARE-dependent (see Fig. 1*B* in Ref. 39). Interestingly, however, the addition of Munc18-1 showed little change in the cumulative time plot in the range of 100–1000 nM, although there was some reduction of content mixing at 1 μM of Munc18-1 (Fig. 4*B*), which is dependent on the Ca^{2+} (Fig. 4*C*). Thus, our result demonstrates that Munc18-1 does not stimulate Ca^{2+}-triggered fusion pore opening, suggesting that the SNAREpin is not accessible to Munc18-1 in the presence of Syt1.

Similarly, we also note that in this assay, the vesicle docking became significantly reduced as the Munc18-1 concentration was increased (Fig. 4*D* and Table 1). We interpret the reducing of vesicle docking as the consequence of dissociation of heterodimeric t-SNARE into the individual components syntaxin-1a and SNAP-25 (30, 49), which would reduce vesicle docking mediated by the interaction between Syt1 and t-SNARE (35, 38). Therefore, it appears that Munc18-1 has the ability to both improve and prevent SNARE complex formation in a concentration-dependent manner.

TABLE 1

Numbers of docked vesicles for content mixing using sulforhodamine B

	Total docked vesicles
SNAREs/Syt1	1466
SNAREs/Syt1, Munc18-1 (100 nM)	769
SNAREs/Syt1, Munc18-1 (200 nM)	560
SNAREs/Syt1, Munc18-1 (500 nM)	547
SNAREs/Syt1, Munc18-1 (1000 nM)	365
SNAREs/Syt1, Munc18-1 (1500 nM)	131

DISCUSSION

In this work, we observed, using smFRET and single vesicle lipid mixing, that the positive influence of Munc18-1 on SNARE zippering and lipid mixing is robust in the absence of Syt1. Our results are consistent with those of Rothman and co-workers (12) and show that Munc18-1 indeed has the capacity to drive the completion of SNARE zippering by acting on the partially zipped (N-terminally assembled but C-terminally frayed) SNARE complex. Rothman and co-workers (12) also showed that the incubation at low temperature, which presumably promotes N-terminal zippering of SNAREs, is required for the enhancement of SNARE-dependent lipid mixing by Munc18-1, again consistent with our results from smFRET on the *trans*-SNAREpin between two apposed nanodiscs.

Surprisingly, however, when Syt1 is present, the stimulation of SNARE zippering by Munc18-1 disappears completely, whereas its effect on lipid mixing is reduced significantly. Most importantly, we did not observe any acceleration of content mixing (or fusion pore opening) by Munc18-1. These findings suggest that Syt1 competes with Munc18-1 for the access to the

SNAREpin and acts as an antagonist for Munc18-1 in SNAREpin binding. It is not clear whether Syt1 binds the SNARE complex in replacement of Munc18-1. We cannot rule out the possibility that Syt1 binds to lipids (most likely PIP_2) in the close vicinity of SNARE complex, which in turn expel Munc18-1 from the SNARE complex. However, it has been shown that Munc18-1 could stimulate lipid mixing in the presence of Syt1 in the recent work employing small/giant unilamellar vesicles (50, 51), even without preincubation on ice. These results appear to be at odds with our data, warranting further investigation.

Neurotransmitter release is tightly regulated by Ca^{2+} and happens in less than 1 ms upon Ca^{2+} influx (52, 53). Thus, it appears to be necessary for Ca^{2+} sensor Syt1 to gain intimate access to the SNAREpin (32). In fact, it is shown that Syt1 has the capacity to bind the SNARE core and negatively charged lipids clustered in the immediate vicinity of the SNARE complex (38, 54).

With the necessity for the presence of Syt1 at the nearest neighbor of the SNAREpin, it is hard to envision how Munc18-1 gains full access to the SNAREpin simultaneously. Meanwhile, Munc18-1 binding to the SNARE core is relatively weak, with a binding constant of $\sim$1 μM (55), which may not be sufficiently strong to hold onto the SNARE core in competition with Syt1.

Alternatively, Munc18-1 binding to the Habc domain of syntaxin-1a is much stronger, with a binding constant of $\sim$10 nM (28, 56). This binding stabilizes the "closed" form of syntaxin-1a, which does not allow the premature binding of syntaxin-1a to SNAP-25 (30). A controlled binding between syntaxin-1a and SNAP-25 is necessary because their free binding probably leads to the formation of the 2:1 complex, which is known to be the non-productive dead end product (57, 58). Recently, it was shown that Munc13 plays a role in relieving syntaxin-1a from the inhibitory Munc18-1 capping (29, 30).

The notion that Munc18-1 is part of the minimal fusion machinery is largely based on two experimental observations. First, the knock-out of Munc18-1 abolishes neurotransmitter release completely (35, 59, 60). The severity of the knock-out phenotype could be explained equally well by the losing of inhibitory capping on syntaxin-1a. Second, Munc18-1 has the capacity of accelerating SNARE-dependent proteoliposome fusion significantly (12, 25). However, the caveat here is that Syt1 is not included in those experiments. Our results argue that Munc18-1 may not be part of the minimal fusion machinery and that it instead plays an important regulatory role in controlling the syntaxin-1a binding to SNAP-25, at least in neuroexocytosis.

There are, however, many exocytotic systems where vesicle fusion is not regulated by Ca^{2+} and Syt1-like molecules (61, 62). Also, there are systems where the Habc-like domain is not present in syntaxin-1a analogs (63, 64). In such cases, the main function of Sec1/Munc18 may be to stimulate vesicle fusion via its binding to the SNAREpin. The analysis by Shen *et al.* (25) suggests that the SNAREpin binding may be the evolutionarily conserved function for the Sec1/Munc18 family. However, at the top of the evolution may be neuroexocytosis. Thus, we speculate that the evolutionary pressure to implement the tight Ca^{2+} control of vesicle fusion might have diverted the role of Munc18-1 elsewhere.

Acknowledgment—We thank Dr. Taekjip Ha (University of Illinois) for providing the analysis program for the single vesicle assay.

REFERENCES

1. Chernomordik, L. V., and Kozlov, M. M. (2003) Protein-lipid interplay in fusion and fission of biological membranes. *Annu. Rev. Biochem.* **72,** 175–207
2. Martens, S., and McMahon, H. T. (2008) Mechanisms of membrane fusion: disparate players and common principles. *Nat. Rev. Mol. Cell Biol.* **9,** 543–556
3. Maximov, A., Tang, J., Yang, X., Pang, Z. P., and Südhof, T. C. (2009) Complexin controls the force transfer from SNARE complexes to membranes in fusion. *Science* **323,** 516–521
4. Rizo, J., and Südhof, T. C. (2012) The membrane fusion enigma: SNAREs, Sec1/Munc18 proteins, and their accomplices: guilty as charged? *Annu. Rev. Cell Dev. Biol.* **28,** 279–308
5. Söllner, T., Whiteheart, S. W., Brunner, M., Erdjument-Bromage, H., Geromanos, S., Tempst, P., and Rothman, J. E. (1993) SNAP receptors implicated in vesicle targeting and fusion. *Nature* **362,** 318–324
6. Sutton, R. B., Fasshauer, D., Jahn, R., and Brunger, A. T. (1998) Crystal structure of a SNARE complex involved in synaptic exocytosis at 2.4 Å resolution. *Nature* **395,** 347–353
7. Poirier, M. A., Xiao, W., Macosko, J. C., Chan, C., Shin, Y. K., and Bennett, M. K. (1998) The synaptic SNARE complex is a parallel four-stranded helical bundle. *Nat. Struct. Biol.* **5,** 765–769
8. Weber, T., Zemelman, B. V., McNew, J. A., Westermann, B., Gmachl, M., Parlati, F., Söllner, T. H., and Rothman, J. E. (1998) SNAREpins: minimal machinery for membrane fusion. *Cell* **92,** 759–772
9. Brunger, A. T. (2005) Structure and function of SNARE and SNARE-interacting proteins. *Q. Rev. Biophys.* **38,** 1–47
10. Jahn, R., and Scheller, R. H. (2006) SNAREs: engines for membrane fusion. *Nat. Rev. Mol. Cell Biol.* **7,** 631–643
11. Stein, A., Weber, G., Wahl, M. C., and Jahn, R. (2009) Helical extension of the neuronal SNARE complex into the membrane. *Nature* **460,** 525–528
12. Shen, J., Tareste, D. C., Paumet, F., Rothman, J. E., and Melia, T. J. (2007) Selective activation of cognate SNAREpins by Sec1/Munc18 proteins. *Cell* **128,** 183–195
13. Deák, F., Xu, Y., Chang, W. P., Dulubova, I., Khvotchev, M., Liu, X., Südhof, T. C., and Rizo, J. (2009) Munc18-1 binding to the neuronal SNARE complex controls synaptic vesicle priming. *J. Cell Biol.* **184,** 751–764
14. Diao, J., Su, Z., Lu, X., Yoon, T. Y., Shin, Y. K., and Ha, T. (2010) Single-vesicle fusion assay reveals Munc18-1 binding to the SNARE core is sufficient for stimulating membrane fusion. *ACS Chem. Neurosci.* **1,** 168–174
15. Schiavo, G., Benfenati, F., Poulain, B., Rossetto, O., Polverino de Laureto, P., DasGupta, B. R., and Montecucco, C. (1992) Tetanus and botulinum-B neurotoxins block neurotransmitter release by proteolytic cleavage of synaptobrevin. *Nature* **359,** 832–835
16. Blasi, J., Chapman, E. R., Link, E., Binz, T., Yamasaki, S., De Camilli, P., Südhof, T. C., Niemann, H., and Jahn, R. (1993) *Botulinum neurotoxin* A selectively cleaves the synaptic protein SNAP-25. *Nature* **365,** 160–163
17. Keller, J. E., and Neale, E. A. (2001) The role of the synaptic protein snap-25 in the potency of botulinum neurotoxin type A. *J. Biol. Chem.* **276,** 13476–13482
18. Breidenbach, M. A., and Brunger, A. T. (2005) New insights into clostridial neurotoxin-SNARE interactions. *Trends Mol. Med.* **11,** 377–381
19. Pobbati, A. V., Stein, A., and Fasshauer, D. (2006) N- to C-terminal SNARE complex assembly promotes rapid membrane fusion. *Science* **313,** 673–676
20. Bhalla, A., Chicka, M. C., Tucker, W. C., and Chapman, E. R. (2006) Ca^{2+}-synaptotagmin directly regulates t-SNARE function during reconstituted membrane fusion. *Nat. Struct. Mol. Biol.* **13,** 323–330
21. Stein, A., Radhakrishnan, A., Riedel, D., Fasshauer, D., and Jahn, R. (2007) Synaptotagmin activates membrane fusion through a Ca^{2+}-dependent

trans interaction with phospholipids. *Nat. Struct. Mol. Biol.* **14,** 904–911
22. Yoon, T. Y., Lu, X., Diao, J., Lee, S. M., Ha, T., and Shin, Y. K. (2008) Complexin and Ca^{2+} stimulate SNARE-mediated membrane fusion. *Nat. Struct. Mol. Biol.* **15,** 707–713
23. Lee, H. K., Yang, Y., Su, Z., Hyeon, C., Lee, T. S., Lee, H. W., Kweon, D. H., Shin, Y. K., and Yoon, T. Y. (2010) Dynamic Ca^{2+}-dependent stimulation of vesicle fusion by membrane-anchored synaptotagmin 1. *Science* **328,** 760–763
24. Shi, L., Shen, Q. T., Kiel, A., Wang, J., Wang, H. W., Melia, T. J., Rothman, J. E., and Pincet, F. (2012) SNARE proteins: one to fuse and three to keep the nascent fusion pore open. *Science* **335,** 1355–1359
25. Yu, H., Rathore, S. S., Lopez, J. A., Davis, E. M., James, D. E., Martin, J. L., and Shen, J. (2013) Comparative studies of Munc18c and Munc18-1 reveal conserved and divergent mechanisms of Sec1/Munc18 proteins. *Proc. Natl. Acad. Sci. U.S.A.* **110,** E3271–E3280
26. Fernandez, I., Ubach, J., Dulubova, I., Zhang, X., Südhof, T. C., and Rizo, J. (1998) Three-dimensional structure of an evolutionarily conserved N-terminal domain of syntaxin 1A. *Cell* **94,** 841–849
27. Dulubova, I., Sugita, S., Hill, S., Hosaka, M., Fernandez, I., Südhof, T. C., and Rizo, J. (1999) A conformational switch in syntaxin during exocytosis: role of munc18. *EMBO J.* **18,** 4372–4382
28. Misura, K. M., Scheller, R. H., and Weis, W. I. (2000) Three-dimensional structure of the neuronal-Sec1-syntaxin 1a complex. *Nature* **404,** 355–362
29. Ma, C., Li, W., Xu, Y., and Rizo, J. (2011) Munc13 mediates the transition from the closed syntaxin-Munc18 complex to the SNARE complex. *Nat. Struct. Mol. Biol.* **18,** 542–549
30. Ma, C., Su, L., Seven, A. B., Xu, Y., and Rizo, J. (2013) Reconstitution of the vital functions of Munc18 and Munc13 in neurotransmitter release. *Science* **339,** 421–425
31. Fernández-Chacón, R., Königstorfer, A., Gerber, S. H., García, J., Matos, M. F., Stevens, C. F., Brose, N., Rizo, J., Rosenmund, C., and Südhof, T. C. (2001) Synaptotagmin I functions as a calcium regulator of release probability. *Nature* **410,** 41–49
32. Chapman, E. R. (2002) Synaptotagmin: a Ca^{2+} sensor that triggers exocytosis? *Nat. Rev. Mol. Cell Biol.* **3,** 498–508
33. Rizo, J., and Rosenmund, C. (2008) Synaptic vesicle fusion. *Nat. Struct. Mol. Biol.* **15,** 665–674
34. Perin, M. S., Brose, N., Jahn, R., and Südhof, T. C. (1991) Domain structure of synaptotagmin (p65). *J. Biol. Chem.* **266,** 623–629
35. de Wit, H., Walter, A. M., Milosevic, I., Gulyás-Kovács, A., Riedel, D., Sørensen, J. B., and Verhage, M. (2009) Synaptotagmin-1 docks secretory vesicles to syntaxin-1/SNAP-25 acceptor complexes. *Cell* **138,** 935–946
36. Hui, E., Johnson, C. P., Yao, J., Dunning, F. M., and Chapman, E. R. (2009) Synaptotagmin-mediated bending of the target membrane is a critical step in Ca^{2+}-regulated fusion. *Cell* **138,** 709–721
37. Lai, Y., and Shin, Y. K. (2012) The importance of an asymmetric distribution of acidic lipids for synaptotagmin 1 function as a Ca^{2+} sensor. *Biochem. J.* **443,** 223–229
38. Kim, J. Y., Choi, B. K., Choi, M. G., Kim, S. A., Lai, Y., Shin, Y. K., and Lee, N. K. (2012) Solution single-vesicle assay reveals PIP2-mediated sequential actions of synaptotagmin-1 on SNAREs. *EMBO J.* **31,** 2144–2155
39. Lai, Y., Lou, X., Jho, Y., Yoon, T. Y., and Shin, Y. K. (2013) The synaptotagmin 1 linker may function as an electrostatic zipper that opens for docking but closes for fusion pore opening. *Biochem. J.* **456,** 25–33
40. Shin, Y. K. (2013) Two gigs of Munc18 in membrane fusion. *Proc. Natl. Acad. Sci. U.S.A.* **110,** 14116–14117
41. Shin, J., Lou, X., Kweon, D. H., and Shin, Y. K. (2014) Multiple conformations of a single SNAREpin between two nanodisc membranes reveal diverse pre-fusion states. *Biochem. J.* **459,** 95–102
42. Kyoung, M., Zhang, Y., Diao, J., Chu, S., and Brunger, A. T. (2013) Studying calcium-triggered vesicle fusion in a single vesicle-vesicle content and lipid-mixing system. *Nat. Protoc.* **8,** 1–16
43. Lai, Y., Diao, J., Liu, Y., Ishitsuka, Y., Su, Z., Schulten, K., Ha, T., and Shin, Y. K. (2013) Fusion pore formation and expansion induced by Ca^{2+} and synaptotagmin 1. *Proc. Natl. Acad. Sci. U.S.A.* **110,** 1333–1338
44. Lai, Y., Lou, X., Wang, C., Xia, T., and Tong, J. (2014) Synaptotagmin 1 and Ca^{2+} drive trans SNARE zippering. *Sci. Rep.* **4,** 4575
45. Roy, R., Hohng, S., and Ha, T. (2008) A practical guide to single-molecule FRET. *Nat. Methods* **5,** 507–516
46. Diao, J., Ishitsuka, Y., Lee, H., Joo, C., Su, Z., Syed, S., Shin, Y. K., Yoon, T. Y., and Ha, T. (2012) A single vesicle-vesicle fusion assay for *in vitro* studies of SNAREs and accessory proteins. *Nat. Protoc.* **7,** 921–934
47. Dulubova, I., Khvotchev, M., Liu, S., Huryeva, I., Südhof, T. C., and Rizo, J. (2007) Munc18-1 binds directly to the neuronal SNARE complex. *Proc. Natl. Acad. Sci. U.S.A.* **104,** 2697–2702
48. Weninger, K., Bowen, M. E., Chu, S., and Brunger, A. T. (2003) Single-molecule studies of SNARE complex assembly reveal parallel and antiparallel configurations. *Proc. Natl. Acad. Sci. U.S.A.* **100,** 14800–14805
49. Zhang, Y., Diao, J., Colbert, K. N., Lai, Y., Pfuetzner, R. A., Padolina, M. S., Vivona, S., Ressl, S., Cipriano, D. J., Choi, U. B., Shah, N., Weis, W. I., and Brunger, A. T. (2015) Munc18a does not alter fusion rates mediated by neuronal SNAREs, synaptotagmin, and complexin. *J. Biol. Chem.* 10.1074/jbc.M114.630772
50. Parisotto, D., Malsam, J., Scheutzow, A., Krause, J. M., and Söllner, T. H. (2012) SNAREpin assembly by Munc18-1 requires previous vesicle docking by synaptotagmin 1. *J. Biol. Chem.* **287,** 31041–31049
51. Parisotto, D., Pfau, M., Scheutzow, A., Wild, K., Mayer, M. P., Malsam, J., Sinning, I., and Söllner, T. H. (2014) An extended helical conformation in domain 3a of Munc18-1 provides a template for SNARE (soluble *N*-ethylmaleimide-sensitive factor attachment protein receptor) complex assembly. *J. Biol. Chem.* **289,** 9639–9650
52. Borst, J. G., and Sakmann, B. (1996) Calcium influx and transmitter release in a fast CNS synapse. *Nature* **383,** 431–434
53. Jahn, R., and Fasshauer, D. (2012) Molecular machines governing exocytosis of synaptic vesicles. *Nature* **490,** 201–207
54. Honigmann, A., van den Bogaart, G., Iraheta, E., Risselada, H. J., Milovanovic, D., Mueller, V., Müllar, S., Diederichsen, U., Fasshauer, D., Grubmüller, H., Hell, S. W., Eggeling, C., Kühnel, K., and Jahn, R. (2013) Phosphatidylinositol 4,5-bisphosphate clusters act as molecular beacons for vesicle recruitment. *Nat. Struct. Mol. Biol.* **20,** 679–686
55. Xu, Y., Su, L., and Rizo, J. (2010) Binding of Munc18-1 to synaptobrevin and to the SNARE four-helix bundle. *Biochemistry* **49,** 1568–1576
56. Burkhardt, P., Hattendorf, D. A., Weis, W. I., and Fasshauer, D. (2008) Munc18a controls SNARE assembly through its interaction with the syntaxin N-peptide. *EMBO J.* **27,** 923–933
57. Fasshauer, D., Otto, H., Eliason, W. K., Jahn, R., and Brünger, A. T. (1997) Structural changes are associated with soluble *N*-ethylmaleimide-sensitive fusion protein attachment protein receptor complex formation. *J. Biol. Chem.* **272,** 28036–28041
58. Xiao, W., Poirier, M. A., Bennett, M. K., and Shin, Y. K. (2001) The neuronal t-SNARE complex is a parallel four-helix bundle. *Nat. Struct. Biol.* **8,** 308–311
59. Verhage, M., Maia, A. S., Plomp, J. J., Brussaard, A. B., Heeroma, J. H., Vermeer, H., Toonen, R. F., Hammer, R. E., van den Berg, T. K., Missler, M., Geuze, H. J., and Südhof, T. C. (2000) Synaptic assembly of the brain in the absence of neurotransmitter secretion. *Science* **287,** 864–869
60. Gerber, S. H., Rah, J. C., Min, S. W., Liu, X., de Wit, H., Dulubova, I., Meyer, A. C., Rizo, J., Arancillo, M., Hammer, R. E., Verhage, M., Rosenmund, C., and Südhof, T. C. (2008) Conformational switch of syntaxin-1 controls synaptic vesicle fusion. *Science* **321,** 1507–1510
61. Schekman, R. (1992) Genetic and biochemical analysis of vesicular traffic in yeast. *Curr. Opin. Cell Biol.* **4,** 587–592
62. Bonifacino, J. S., and Glick, B. S. (2004) The mechanisms of vesicle budding and fusion. *Cell* **116,** 153–166
63. Dulubova, I., Yamaguchi, T., Wang, Y., Südhof, T. C., and Rizo, J. (2001) Vam3p structure reveals conserved and divergent properties of syntaxins. *Nat. Struct. Biol.* **8,** 258–264
64. Dulubova, I., Yamaguchi, T., Gao, Y., Min, S. W., Huryeva, I., Südhof, T. C., and Rizo, J. (2002) How Tlg2p/syntaxin 16 "snares" Vps45. *EMBO J.* **21,** 3620–3631
65. Yoon, T. Y., Okumus, B., Zhang, F., Shin, Y. K., and Ha, T. (2006) Multiple intermediates in SNARE-induced membrane fusion. *Proc. Natl. Acad. Sci. U.S.A.* **103,** 19731–19736